Identification of Killer Defects in Kesterite Thin-Film Solar Cells

Sunghyun Kim,[†] Ji-Sang Park,[†] and Aron Walsh*,[†,‡]

[†]Department of Materials, Imperial College London, London SW7 2AZ, United Kingdom
[‡]Department of Materials Science and Engineering, Yonsei University, Seoul 03722, Korea

S *Supporting Information*

ABSTRACT: Nonradiative electron−hole recombination is the bottleneck to efficient kesterite thin-film solar cells. We have performed a search for active point defect recombination centers using first-principles calculations. We show that the anion vacancy in Cu_2ZnSnS_4 (CZTS) is electrically benign without a donor level in the band gap. V_S can still act as an efficient nonradiative site through the aid of an intermediate excited state involving electron capture by Sn. The bipolaron associated with Sn^{4+} to Sn^{2+} two-electron reduction stabilizes the neutral sulfur vacancy over the charged states; however, we demonstrate a mechanism whereby nonradiative recombination can occur via multiphonon emission. Our study highlights that defect-mediated recombination does *not* require a charge transition level deep in the band gap of a semiconductor. We further identify Sn_{Zn} as the origin of persistent electron trapping/detrapping in kesterite photovoltaic devices, which is suppressed in the selenide compound.
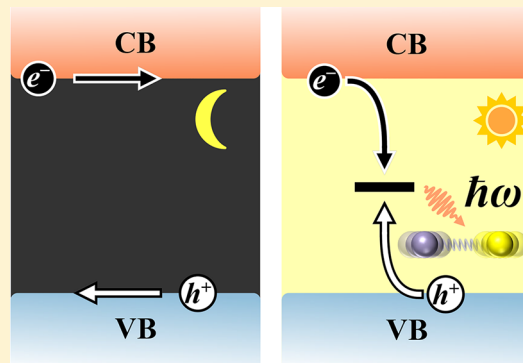
Thin-film solar cells require less materials and energy to produce compared to silicon-based technologies.[1,2] Kesterite-structured tetrahedral semiconductors such as Cu_2ZnSnS_4 (CZTS) and $Cu_2ZnSnSe_4$ (CZTSe), illustrated in Figure 1, have attracted much attention due to the earth-abundance of Cu, Zn, and Sn.[3] Recently, a kesterite solar cell reached a record light-to-electricity conversion efficiency of 12.6%;[4] however, this technology suffers from a large open-circuit voltage (V_{OC}) deficit.[3−6] Thus, the performance of current kesterite-based solar cells falls far below the Shockley−Queisser limit of ∼30%.[7,8] One likely origin of the V_{OC} deficit is an electron−hole recombination center—a so-called killer defect—that limits the minority carrier lifetime.[9]

In the nonradiative recombination process described by Shockley−Read−Hall (SRH)[10,11] statistics, a deep level in the band gap of a semiconductor provides an intermediate state that facilitates the capture of both minority and majority carriers. If the defect level is close to the conduction band, the captured electron is likely to be emitted before recombination occurs. On the other hand, as the defect level approaches the valence band, it becomes increasingly difficult to capture an electron from the conduction band. Therefore, a midgap state is generally considered an efficient SRH recombination center. However, the original model did not take into account the distinct transition levels and atomic relaxation processes associated with different charge states of the same defect, an assumption that has been challenged in subsequent studies.[12−14]

There have been a number of density functional theory (DFT) studies of point defect formation in kesterite materials.[15−22] In CZTS and CZTSe, it has been shown that the defects with low formation energies (e.g., V_{Cu} and Cu_{Zn}) have defect transition levels close to the band edges. In contrast to Cu(I) and Zn(II), the higher valence of Sn(IV) results in deeper levels for Sn-related defects; although, usually these are higher in energy to form. The double donor level $\varepsilon(0/2+)$ of Sn_{Zn} is located near the midgap,[17,19] but it is unlikely to be an efficient recombination center because it requires simultaneous two-electron capture. A microscopic understanding of nonradiative recombination mechanisms in kesterites is still unclear.

In this Letter, we revisit point defect processes in kesterite semiconductors from first-principles. We show that the electrically benign sulfur vacancy (V_S) can play a crucial role in capturing electrons and facilitating nonradiative recombination. Sn reduction (bipolaron formation) stabilizes the neutral V_S in CZTS, where the donor level lies *below* the valence band maximum (VBM). However, V_S can be excited to capture two holes, turning into the doubly charged V_S^{2+}. We find that the electron capture process occurs with a negligible barrier, indicating that V_S provides an efficient nonradiative recombination channel in kesterite semiconductors.

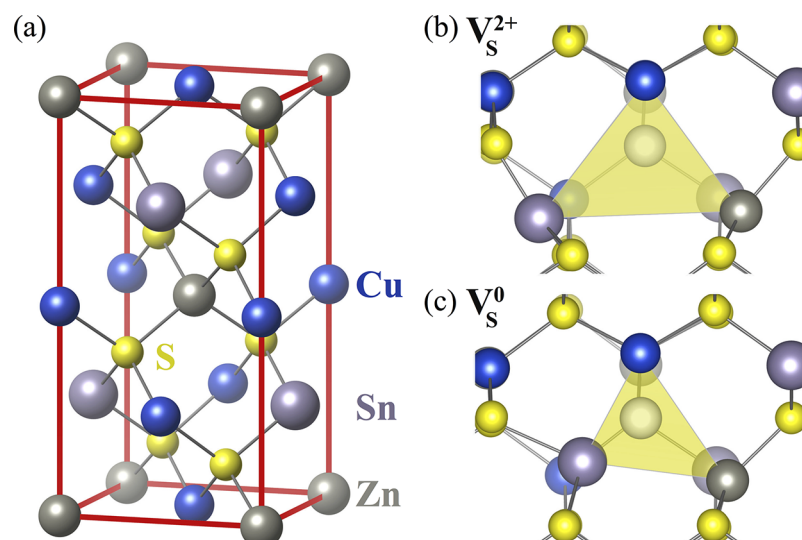Figure 1. (a) Atomic structure of kesterite Cu_2ZnSnS_4 and (b) +2 charged and (c) neutral sulfur vacancies. Blue, gray, purple, yellow, and white balls represent Cu, Zn, Sn, and S atoms and vacancy site, respectively.
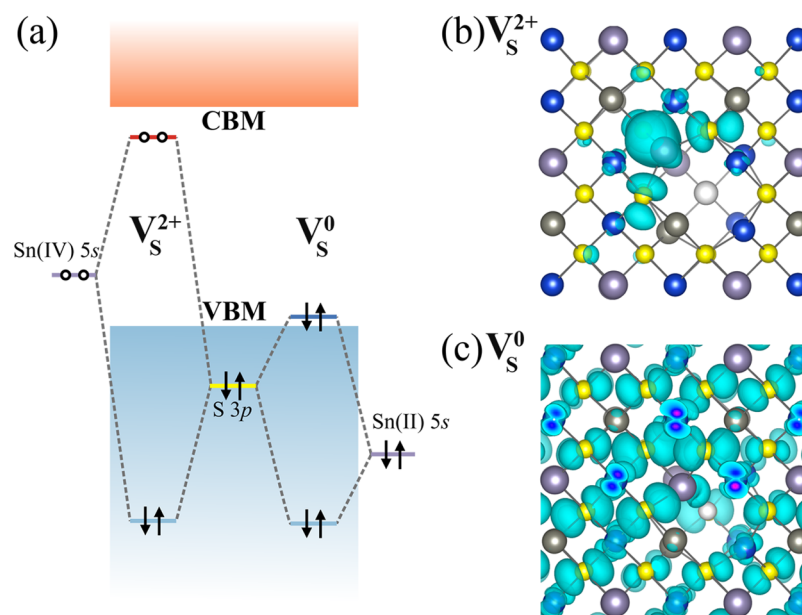

Figure 2. (a) Schematic energy level diagram associated with sulfur vacancy formation. Charge densities of (b) the lowest unoccupied Kohn–Sham state associated with V_S^{2+} and (c) the highest occupied state associated with V_S^0.

The formation energy and electronic structure of a series of point defects were calculated from first-principles within the framework of DFT.[23,24] We employed the projector-augmented wave method[25] and the hybrid exchange–correlation functional of Heyd–Scuseria–Ernzerhof (HSE06),[26] as implemented in VASP.[27] The wave functions were expanded in plane waves up to an energy cutoff of 400 eV. A Monkhorst–Pack k-mesh[28] with a grid spacing less than $2\pi \times 0.03$ Å^{-1} was used for Brillouin zone integration. The atomic coordinates were optimized until the residual forces were less than 0.02 eV/Å. The lattice vectors were relaxed until stress was below 0.5 kbar. For defect formation, a $2 \times 2 \times 1$ supercell expansion (64 atoms) of the conventional cell was employed. For charged defects, potential alignment, and anisotropic electrostatic corrections were applied using the calculated static dielectric tensor.

Anion Vacancy: Stable and Metastable Charge States. Anion vacancies in semiconductors usually act as shallow electron donors or deep recombination centers.[29] In CZTS, each S is coordinated to two Cu, one Zn, and one Sn atom, forming a tetrahedron. A sulfur vacancy results in two excess electrons, which can be donated to the conduction band, resulting in the doubly charged V_S^{2+}. Around V_S^{2+}, all cations undergo an outward distortion; the neighboring Sn atom relaxes by 0.86 Å away from the vacancy site, as shown in Figure 1b.

On the other hand, V_S can also exist in a neutral charge state. The neighboring Sn atom can accommodate two electrons by reducing its valence: $Sn(IV) + 2e^- \rightarrow Sn(II)$. As V_S^{2+} captures two electrons, V_S^0 is formed and the Sn atom relaxes by 1.41 Å toward the vacancy site; see Figure 1c. The remaining Sn–S bond lengths increase by 0.18 Å.

The charge densities of V_S^{2+} and V_S^0 illustrate the double reduction of Sn. We find that the V_S^{2+} produces a deep single-
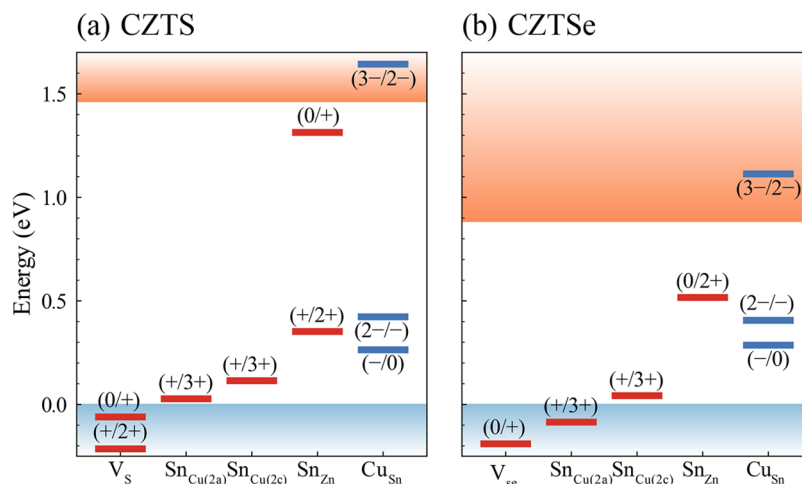
Figure 3. (a) Thermodynamic charge transition levels of V_S, $Sn_{Cu(2a)}$, $Sn_{Cu(2c)}$, Sn_{Zn}, and Cu_{Sn} in (a) Cu_2ZnSnS_4 (CZTS) and (b) $Cu_2ZnSnSe_4$ (CZTSe), calculated using DFT/HSE06 including image charge corrections.
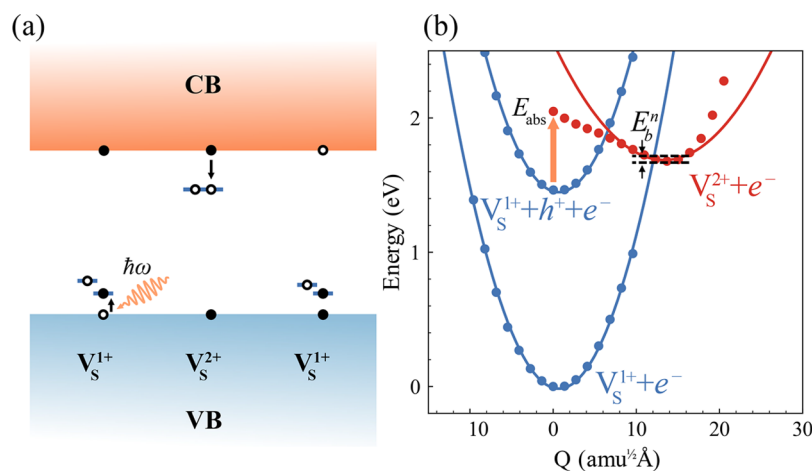

Figure 4. (a) Proposed nonradiative recombination process where a V_S^+ defect is photoactivated into a V_S^{2+} state that facilitates electron capture. (b) Configuration coordinate diagram for the same process; the dots represent calculated points on the potential energy surface, while lines are a parabolic fit. The labels E_{abs} and E_b^n represent the optical excitation and electron capture barrier, respectively.

particle level in the band gap, while a resonant state in the valence band is formed by V_S^0; see Figure 2a. The empty level of V_S^{2+} is localized in the form of an antibonding Sn 5s–S 3p* orbital, Figure 2b. The defect state strongly couples with the valence band and becomes resonant when occupied, as illustrated in Figure 2c. These orbital interactions and local relaxations are common for lone pair formation in ns² post-transition metal compounds.[30]

When V_S^{2+} captures one electron, it becomes a singly-charged sulfur vacancy, V_S^{1+}. The atomic structure of V_S^{1+} is similar to that of V_S^0 with the Sn relaxation of 1.20 Å toward the vacancy site, which is comparable to 1.41 Å of V_S^0. As one electron occupies the Sn 5s–S 3p* orbital, an exchange splitting between spin-up and spin-down states of 23 meV leads to an unpaired electron with the formation of a Sn(III) center.

We examine the thermodynamic transition levels $\epsilon(q1/q2)$ defined as the Fermi level where the formation energies of defects in charge states $q1$ and $q2$ are equal (see the Supporting Information for the phase diagram of CZTS and the formation energies). We include a correction for artificial electrostatic interactions in a charged periodic system.[31,32] The single donor level $\epsilon(0/1+)$ lies 60 meV below the VBM, indicating that V_S^0 is thermodynamically stable for all Fermi-level positions, Figure

3a, consistent with previous calculations.[19,33] Note that the calculated band gap of CZTS is 1.46 eV, while the experimental room-temperature band gap is 1.5 eV.[20] The bipolaron state (two electrons stabilized by lattice polarization[29]) makes V_S electrically inactive with no donor level in the band gap.

Although V_S^{1+} is thermodynamically metastable, the difference in the formation energies of V_S^{1+} and V_S^0 is small. At room temperature, a concentration of ~10% V_S^{1+} is expected from equilibrium thermodynamics. The unoccupied level of V_S^{1+} is close to the valence band; therefore, V_S^{1+} cannot capture an electron efficiently. However, under illumination in a solar cell, V_S^{1+} can capture an additional hole by excitation at $E_{abs} = 0.59$ eV (see Figure 4). Hole capture raises the empty state of V_S^{2+} close to the conduction band. V_S^{2+} can efficiently capture an electron and recover the +1 charge state, thus completing the electron−hole recombination process.

We find that the electron capture process is fast with a negligible barrier. The configuration coordinate diagram is shown in Figure 4b. The significant lattice distortion shifts the potential energy surface (PES) of V_S^{2+} considerably. Because the local minimum of the +2 charge state lies outside of the PES of the +1 charge state, the electron capture process is always nonradiative. The low barrier for the electron capture, $E_b^n = 8$

meV, suggests that the captured holes will rapidly recombine with electrons. On the basis of a static approximation,[13,34,35] the calculated capture coefficient is 3.9×10^{-6} cm^3/s at 300 K. The corresponding capture cross section is 3.9×10^{-13} cm^2 for the thermal velocity of 10^7 cm/s. During the recovery to the ground-state geometry of V_S^{1+}, the potential energy is dissipated via multiphonon emission.

Unlike a conventional nonradiative recombination process, here the minority carrier capture process is fast. Due to the low electron capture barrier, the electron capture coefficient is weakly dependent on the temperature. However, the total recombination rate is expected to exponentially increase because of the thermal excitation of V_S^0 to V_S^{1+}. The overall recombination rate is limited by the population of V_S^{1+} and the photoexcitation from V_S^{1+} to V_S^{2+}. We propose that the photoactivated nonradiative recombination process explains the reduced photoluminescence intensity under extra sub-band gap illumination in CZTS.[36]

Antisites and the Multivalence of Sn. We also examined polaronic solutions for Sn_{Zn}. Sn_{Zn}^{2+} captures two electrons via double Sn reduction. The occupied lone pair of Sn_{Zn}^0 is located 0.36 eV above the valence band. When one electron is removed, there is an exchange splitting of 0.7 eV. The two donor levels, $\epsilon(0/+)$ and $\epsilon(+/2+)$, lay at 0.11 eV below the CBM and 0.35 eV above the VBM, respectively. In contrast to previous calculations,[17,19] the deep level of $\epsilon(0/2+)$ is absent when an open-shell solution for Sn_{Zn}^{1+} is considered.

We find a similar bipolaronic state in Sn_{Cu}, stabilizing Sn_{Cu}^{1+} over Sn_{Cu}^{3+}, as shown in Figure 3a. However, in contrast to Sn_{Zn}, the single electron capture to give Sn_{Cu}^{2+} is unfavorable. The absence of Sn(III) in Sn_{Cu} is due to the difference in the energies of lone pair states of Sn_{Zn} and Sn_{Cu}. The lone pair of Sn_{Cu} is much deeper than that of Sn_{Zn}. Valence electrons screen the electron−electron repulsion (U) of Sn_{Cu} significantly,[37,38] and the effective U becomes negative with the aid of structure relaxation.

On the other hand, Cu antisites can also capture holes via oxidation of Cu. We find that a tetrahedral distortion pushes up one of the t_2 levels of Cu_{Sn}. As shown in Figure 3a, the acceptor level $\epsilon(3-/2-)$ lies above the CBM, implying that the oxidation state of Cu_{Sn} is always higher than +1. We find that the polaronic state in the band gap is well localized around the antibonding combination of the Cu 3d and S 3p orbitals (Cu 3d−S 3p*). CZTS in the kesterite form has two symmetrically distinct Cu sites (2a and 2c); however, the difference in formation energies is small, as shown in Figure 3a.

Role of the Madelung Potential. The stability of charge states, as well as the strength of polaronic trapping of charge carriers, can be related to the site Madelung (electrostatic) potentials of the crystal. The Cu^{1+} (2a and 2c), Zn^{2+} (2d), and Sn^{4+} (2b) lattice sites have screened Madelung potentials of 1.17, 1.20, 1.48, and 2.02 V, respectively. Accordingly, Sn favors less positive charged states when it occupies Cu or Zn sites, giving rise to Sn(III) and even Sn(II). In contrast, Cu_{Sn} feels an increased potential, leading to Cu oxidation.

Source of carrier trapping/detrapping. All Sn and Cu antisite defects are too shallow or too deep to acts as efficient electron−hole recombination centers. Sn_{Zn} has two donor levels in the band gap: $\epsilon(0/+)$ and $\epsilon(+/2+)$. Because $\epsilon(+/2+)$ is close to the valence band, the electron capture barrier for Sn_{Zn}^{2+} is high, about 1 eV. Similarly, we ruled out Sn_{Cu}^{3+} as an efficient nonradiative recombination center. On the contrary, Sn_{Zn}^{1+} can capture an electron with a small barrier, while a hole capture is

unlikely. Thus, we propose Sn_{Zn} as the origin of the observed persistent electron trapping/detrapping in CZTS.[39]

While Sn(III) associated with Sn_{Zn}^{1+} is rarely found due to its unusual electronic configuration with a half-filled 5s orbital ($5s^15p^0$), the presence of Sn(III) in the form of Sn_{Zn}^{1+} or V_S^{1+} is supported by the electron spin resonance signals with small *g*-factor in CZTS,[40] which is identical to that of Sn(III) that has been previously observed in doped samples of ZnS.[41]

Case of Cu$_2$ZnSnSe$_4$. The band gap of the selenide is 0.5 eV smaller than that of the sulfide, which is due to a higher valence band edge associated with Se 3p.[42] This higher anion p state is also known to suppress Sn lone pair formation.[30] For CZTSe, we have performed similar defect calculations and analysis and found similar charge transition levels, as shown in Figure 3b. The $\epsilon(0/1+)$ level of V_{Se} is deeper than that of V_S, indicating that the deep level recombination in CZTSe is less effective. Because Sn_{Zn}^{1+} is unstable in CZTSe, the electron trapping/detrapping is also predicted to be less prevalent. We propose that the absence of Sn(III) in CZTSe partially explains the better photovoltaic efficiency of CZTSe-based devices.[3]

In summary, we have reassessed the point defect process in kesterite semiconductors. The spontaneous two-electron reduction of Sn(IV) to Sn(II) stabilizes the neutral charge state of the sulfur vacancy, without any thermal donor level in the band gap. However, we show that sulfur substoichiometry could still give rise to an active nonradiative carrier recombination assisted by an optically excited state. The proposed recombination mechanism implies that careful control of the chemical potential of S/Se could enhance the minority carrier lifetime. A further prediction of the model is that infrared illumination will significantly reduce the minority carrier lifetime. Finally, we identify Sn_{Zn} as an origin of electron trapping/detrapping in operating solar cells.

■ ASSOCIATED CONTENT

Ⓢ Supporting Information

The Supporting Information is available free of charge on the ACS Publications website at DOI: 10.1021/acsenergy-lett.7b01313.

> Phase diagram of CZTS and formation energies of defects (PDF)

■ AUTHOR INFORMATION

Corresponding Author

*E-mail: a.walsh@imperial.ac.uk.

ORCID ⓘ

Sunghyun Kim: 0000-0001-5072-6801

Ji-Sang Park: 0000-0002-1374-8793

Aron Walsh: 0000-0001-5460-7033

Notes

The authors declare no competing financial interest.

The primary data for this article can be accessed at https://doi.org/10.5281/zenodo.1162659.

■ ACKNOWLEDGMENTS

■ REFERENCES

(1) Hoffert, M. I. Farewell to Fossil Fuels? *Science* **2010**, *329*, 1292.

(2) Polman, A.; Knight, M.; Garnett, E. C.; Ehrler, B.; Sinke, W. C. Photovoltaic Materials: Present Efficiencies and Future Challenges. *Science* **2016**, *352*, aad4424.

(3) Kaur, K.; Kumar, N.; Kumar, M. Strategic Review of Interface Carrier Recombination in Earth abundant Cu−Zn−Sn−S−Se Solar Cells: Current Challenges and Future Prospects. *J. Mater. Chem. A* **2017**, *5*, 3069.

(4) Wang, W.; Winkler, M. T.; Gunawan, O.; Gokmen, T.; Todorov, T. K.; Zhu, Y.; Mitzi, D. B. Device Characteristics of CZTSSe Thin-film Solar Cells with 12.6% Efficiency. *Adv. Energy Mater.* **2014**, *4*, 1301465.

(5) Barkhouse, D. A. R.; Gunawan, O.; Gokmen, T.; Todorov, T. K.; Mitzi, D. B. Device Characteristics of a 10.1% Hydrazine-processed $Cu_2ZnSn(Se,S)_4$ Solar Cell. *Prog. Photovoltaics* **2012**, *20*, 6.

(6) Todorov, T. K.; Tang, J.; Bag, S.; Gunawan, O.; Gokmen, T.; Zhu, Y.; Mitzi, D. B. Beyond 11% Efficiency: Characteristics of State-of-the-art $Cu_2ZnSn(S,Se)_4$ Solar Cells. *Adv. Energy Mater.* **2013**, *3*, 34.

(7) Shockley, W.; Queisser, H. J. Detailed Balance Limit of Efficiency of p-n Junction Solar Cells. *J. Appl. Phys.* **1961**, *32*, 510.

(8) Rühle, S. Tabulated Values of the Shockley−Queisser Limit for Single Junction Solar Cells. *Sol. Energy* **2016**, *130*, 139.

(9) Wallace, S. K.; Mitzi, D. B.; Walsh, A. The Steady Rise of Kesterite Solar Cells. *ACS Energy Lett.* **2017**, *2*, 776.

(10) Hall, R. N. Electron-hole Recombination in Germanium. *Phys. Rev.* **1952**, *87*, 387.

(11) Shockley, W.; Read, W. T. J. Statistics of the Recombinations of Holes and Electrons. *Phys. Rev.* **1952**, *87*, 835.

(12) Gibb, R. M.; Rees, G. J.; Thomas, B. W.; Wilson, B. L. H.; Hamilton, B.; Wight, D. R.; Mott, N. F. V. A Two Stage Model for Deep Level Capture. *Philos. Mag.* **1977**, *36*, 1021.

(13) Alkauskas, A.; Dreyer, C. E.; Lyons, J. L.; Van de Walle, C. G. Role of Excited States in Shockley-Read-Hall Recombination in Wide-band-gap Semiconductors. *Phys. Rev. B: Condens. Matter Mater. Phys.* **2016**, *93*, 201304.

(14) Yang, J.-H.; Shi, L.; Wang, L.-W.; Wei, S.-H. Non-Radiative Carrier Recombination Enhanced by Two-level Process: A First-principles Study. *Sci. Rep.* **2016**, *6*, 835.

(15) Chen, S.; Yang, J.-H.; Gong, X. G.; Walsh, A.; Wei, S.-H. Intrinsic Point Defects and Complexes in the Quaternary Kesterite Semiconductor Cu_2ZnSnS_4. *Phys. Rev. B: Condens. Matter Mater. Phys.* **2010**, *81*, 245204.

(16) Nagoya, A.; Asahi, R.; Wahl, R.; Kresse, G. Defect Formation and Phase Stability of Cu_2ZnSnS_4 Photovoltaic Material. *Phys. Rev. B: Condens. Matter Mater. Phys.* **2010**, *81*, 113202.

(17) Biswas, K.; Lany, S.; Zunger, A. The Electronic Consequences of Multivalent Elements in Inorganic Solar Absorbers: Multivalency of Sn in Cu_2ZnSnS_4. *Appl. Phys. Lett.* **2010**, *96*, 201902.

(18) Chen, S.; Walsh, A.; Gong, X.-G.; Wei, S.-H. Classification of Lattice Defects in the Kesterite Cu_2ZnSnS_4 and $Cu_2ZnSnSe_4$ Earth-abundant Solar Cell Absorbers. *Adv. Mater.* **2013**, *25*, 1522.

(19) Han, D.; Sun, Y. Y.; Bang, J.; Zhang, Y. Y.; Sun, H.-B.; Li, X.-B.; Zhang, S. B. Deep Electron Traps and Origin of p-type Conductivity in the Earth-abundant Solar-cell Material Cu_2ZnSnS_4. *Phys. Rev. B: Condens. Matter Mater. Phys.* **2013**, *87*, 155206.

(20) Scragg, J. J. S.; Larsen, J. K.; Kumar, M.; Persson, C.; Sendler, J.; Siebentritt, S.; Platzer-Björkman, C. Cu-Zn Disorder and Band Gap Fluctuations in $Cu_2ZnSn(S,Se)_4$: Theoretical and Experimental Investigations. *Phys. Status Solidi B* **2016**, *253*, 247.

(21) Yee, Y. S.; Magyari-Kope, B.; Nishi, Y.; Bent, S. F.; Clemens, B. M. Deep Recombination Centers in $Cu_2ZnSnSe_4$ Revealed by Screened-exchange Hybrid Density Functional Theory. *Phys. Rev. B: Condens. Matter Mater. Phys.* **2015**, *92*, 195201.

(22) Yu, K.; Carter, E. A. Determining and Controlling the Stoichiometry of Cu_2ZnSnS_4 Photovoltaics: The Physics and Its Implications. *Chem. Mater.* **2016**, *28*, 4415.

(23) Hohenberg, P.; Kohn, W. Inhomogeneous Electron Gas. *Phys. Rev.* **1964**, *136*, B864.

(24) Kohn, W.; Sham, L. J. Self-consistent Equations Including Exchange and Correlation Effects. *Phys. Rev.* **1965**, *140*, A1133.

(25) Blöchl, P. E. Projector Augmented-wave Method. *Phys. Rev. B: Condens. Matter Mater. Phys.* **1994**, *50*, 17953.

(26) Heyd, J.; Scuseria, G. E.; Ernzerhof, M. Hybrid Functionals Based on a Screened Coulomb Potential. *J. Chem. Phys.* **2003**, *118*, 8207.

(27) Kresse, G.; Joubert, D. From Ultrasoft Pseudopotentials to the Projector Augmented-wave Method. *Phys. Rev. B: Condens. Matter Mater. Phys.* **1999**, *59*, 1758.

(28) Monkhorst, H. J.; Pack, J. D. Special Points for Brillouin-zone Integrations. *Phys. Rev. B* **1976**, *13*, 5188.

(29) Stoneham, A. M. *Theory of Defects in Dolids*; Oxford University Press: Oxford, U.K., 1975.

(30) Walsh, A.; Payne, D. J.; Egdell, R. G.; Watson, G. W. Stereochemistry of Post-transition Metal Oxides: Revision of the Classical Lone Pair Model. *Chem. Soc. Rev.* **2011**, *40*, 4455.

(31) Freysoldt, C.; Neugebauer, J.; Van de Walle, C. G. Fully Ab Initio Finite-size Corrections for Charged-defect Supercell Calculations. *Phys. Rev. Lett.* **2009**, *102*, 016402.

(32) Kumagai, Y.; Oba, F. Electrostatics-based Finite-size Corrections for First-principles Point Defect Calculations. *Phys. Rev. B: Condens. Matter Mater. Phys.* **2014**, *89*, 195205.

(33) Zhang, X.; Han, M.; Zeng, Z.; Lin, H. Q. The Instability of S Vacancies in Cu_2ZnSnS_4. *RSC Adv.* **2016**, *6*, 15424.

(34) Alkauskas, A.; Yan, Q.; Van de Walle, C. G. First-principles Theory of Nonradiative Carrier Capture via Multiphonon Emission. *Phys. Rev. B: Condens. Matter Mater. Phys.* **2014**, *90*, 27.

(35) Alkauskas, A.; McCluskey, M. D.; Van de Walle, C. G. Tutorial: Defects in Semiconductors? Combining Experiment and Theory. *J. Appl. Phys.* **2016**, *119*, 181101.

(36) Halim, M. A.; Islam, M. M.; Luo, X.; Xu, C.; Sakurai, T.; Sakai, N.; Kato, T.; Sugimoto, H.; Tampo, H.; Shibata, H.; et al.. *Study of recombination process in Cu_2ZnSnS_4 thin film using two-wavelength excited photoluminescence*; IEEE 40th Photovoltaic Specialists Conference (PVSC), Denver, CO, 2014; p 2334.

(37) Haldane, F. D. M.; Anderson, P. W. Simple Model of Multiple Charge States oF Transition-metal Impurities in Semiconductors. *Phys. Rev. B* **1976**, *13*, 2553.

(38) Raebiger, H.; Lany, S.; Zunger, A. Charge Self-regulation upon Changing the Oxidation State of Transition Metals in Insulators. *Nature* **2008**, *453*, 763.

(39) Hages, C. J.; Redinger, A.; Levcenko, S.; Hempel, H.; Koeper, M. J.; Agrawal, R.; Greiner, D.; Kaufmann, C. A.; Unold, T. Identifying the Real Minority Carrier Lifetime in Nonideal Semiconductors: A Case Study of Kesterite Materials. *Adv. Energy Mater.* **2017**, *7*, 1700167.

(40) Chory, C.; Zutz, F.; Witt, F.; Borchert, H.; Parisi, J. Synthesis and Characterization of Cu_2ZnSnS_4. *Phys. Status Solidi C* **2010**, *7*, 1486.

(41) Backs, D.; Freyer, H. J. Photosensitive EPR of Ge^{3+} and Sn^{3+} in Twinned Cubic Zinc Sulfide. *Phys. Status Solidi B* **1982**, *111*, 117.

(42) Chen, S.; Walsh, A.; Yang, J.-H.; Gong, X. G.; Sun, L.; Yang, P.-X.; Chu, J.-H.; Wei, S.-H. Compositional Dependence of Structural and Electronic Properties of $Cu_2ZnSn(S,Se)_4$ Alloys for Thin Film Solar Cells. *Phys. Rev. B: Condens. Matter Mater. Phys.* **2011**, *83*, 125201.